Research Article

Journal of RAMAN SPECTROSCOPY

Received: 12 April 2011 Revised: 6 July 2011 Accepted: 16 July 2011 Published online in Wiley Online Library: 27 October 2011

(wileyonlinelibrary.com) DOI 10.1002/jrs.3049

Raman investigation of hydrostatic and nonhydrostatic compressions of OH- and F-apophyllites up to 8 GPa

Sergei V. Goryainov,[a,b,c]* Alexander S. Krylov,[d] Yuanming Pan,[b] Iliya A. Madyukov,[a] Mikhail B. Smirnov[e] and Alexander N. Vtyurin[d]

Layer silicates F- and OH-apophyllites, $KCa_4Si_8O_{20}(F, OH)\cdot 8H_2O$, have been investigated by Raman spectroscopy at hydrostatic and nonhydrostatic pressures up to ~8 GPa in diamond anvil cells using a 4 : 1 methanol–ethanol mix as pressure-transmitting medium. Our experiments show that at hydrostatic compression, apophyllites retain their crystalline states (i.e. no amorphization) up to 5 GPa. The wavenumbers of most bands exhibit linear dependences on pressure, except for a few ones, e.g. at 162 and 3565 cm^{-1} in OH-form (160.5 and 3558 cm^{-1} in F-form) that show nonlinear dependences. Nonhydrostatic compression with additional uniaxial loading induces amorphization of apophyllites. The majority of the bands in OH-apophyllite decreases markedly in intensity and shows considerable broadening under nonhydrostatic compression up to 3–6 GPa. In addition, the wavenumbers of several bands at nonhydrostatic compression exhibit considerable nonlinear dependences on pressure with strong hysteresis. These bands are mainly associated with vibrations of the interlayer ions and molecules and also of stretching and bending silicate sheets, hence being highly sensitive to the interlayer distance. Finally, we have calculated the lattice dynamics of F-apophyllite and interpreted the majority of bands, and these data are used to explain the complex baric behavior of the bands. Copyright © 2011 John Wiley & Sons, Ltd.

Keywords: Raman spectroscopy; high pressure; apophyllite; layer silicate; amorphization

Introduction

The study of nonhydrostatic compression influence upon materials is important for understanding their stability at nonhydrostatic mechanical stress. For example, nonisotropic and shear mechanical stresses appear when exploiting materials for building constructions. On the other hand, natural minerals are also affected by nonisotropic and shear mechanical stresses in subduction zones and other tectonic settings.

Investigation of hydrostatic and nonhydrostatic compression of α-quartz led to the understanding that compressed materials expose different transformations at varied deviations from hydrostacity. *Ab initio* calculations and experimental studies of α-quartz confirmed the different paths of structural transformations at varied nonhydrostatic conditions described by mechanical stress tensor σ_{ij}; nonhydrostatic compression leads to transition into quartz II,[1] which is not observed at highly hydrostatic compression in the helium medium.[2,3] Additionally, nonhydrostatic conditions promote the amorphization of α-quartz, decreasing the transition pressure to the amorphous state that is observed simultaneously with quartz II.[4]

Calculations proved the appearance of 5-coordinated Si atoms in crystalline and amorphous HP-phases of quartz:[1,5] quartz II with 5-coordinated Si forms at strong nonhydrostacity $\Delta\sigma_{ii}/\sigma_{xx} \sim 0.3$ and higher ($\Delta\sigma_{ii} = \sigma_{zz} - \sigma_{yy}$). Namely, nonhydrostatic compression up to $\sigma_{xx} = \sigma_{yy} = 20$ GPa and $\sigma_{zz} = 30$ GPa induces this crystalline phase of content: 100%Si^{V}, 50%O^{II}, 50%O^{III}.

Calculations of quartz behavior at effective pressures lower than $\sigma_{ii} \sim 35$ GPa showed the absence of any crystalline phase with 6-coordinated Si (no stishovite or others). Note that at hydrostatic compression α-quartz transforms to the amorphous phase containing Si^{IV} and Si^{V}, but crystalline quartz II does not appear. Complex amorphization processes were observed in quartz-like materials.[5–7]

Some effects of nonhydrostatic compression were investigated using experiments with dry powders in the absence of any *P*-transmitting medium. Kleppe and Jephcoat considered such condition as the extreme case of nonhydrostacity.[8] We suggest that applying the combined loading (hydrostatic + uniaxia stress) better represents natural mechanical stresses (static compression in Earth's depth and the gravity field)

* *Correspondence to: Sergei V. Goryainov, Institute of Geology and Mineralogy SB RAS, pr. Koptyug 3, Novosibirsk 630090, Russia. E-mails: svg@igm.nsc.ru, goryainov@ngs.ru*

a *Institute of Geology and Mineralogy SB RAS, pr. Koptyug 3, Novosibirsk 630090, Russia*

b *Department of Geological Sciences, University of Saskatchewan, Saskatoon SK S7N 5E2, Canada*

c *Novosibirsk State University, Pirogov st., 2, Novosibirsk 630090, Russia*

d *Kirensky Institute of Physics SB RAS, Krasnoyarsk 660036, Russia*

e *Faculty of Physics, St. Petersburg State University, Ulyanovskaya st., 3, St. Petersburg 198504, Russia*

inside lithosphere slabs, in subduction zones and other seismically active regions. On the other hand, studies of nonhydrostatic compression effects on the static and dynamic (vibrational) structure of minerals are scarce.

Various minerals are often used as components of composite building materials and ceramics. Apophyllites are considered as a prospective material for these purposes. Natural apophyllites $KCa_4Si_8O_{20}(F,OH) \cdot 8H_2O$ often have mixed OH–F compositions. OH-apophyllite containing both molecular water and the hydroxyl group is a layered phyllosilicate with high *P–T* stability.[9,10]

Apophyllites have a lot of properties similar to zeolite-group minerals, but their principal dehydration behavior is different. For example, apophyllites have no ability to re-absorb water like zeolites. Apophyllites and zeolites often occur together in low temperature/low pressure metamorphic environments, particularly in cavities of hydrothermally altered basalts and similar rocks. Other commonly associated minerals include pectolite and calcite. Therefore, the study of apophyllites is also important for modeling of post-magmatic processes.

The tetragonal ($P4/mnc = D^6_{4h}$, $Z = 2$) crystal structure of apophyllite $KCa_4Si_8O_{20}(F,OH) \cdot 8H_2O$ is composed of tetrahedral silicate sheets linked together by layers of Ca^{2+} cations and K^+–F^-/OH^- cation–anion pairs (Fig. 1).[11] Silicate sheets contain one type of tetrahedral site, T = Si. Cell parameters of F-apophyllite are $a = b = 8.960$ Å, $c = 15.78$ Å.[11]

There are charged tail atoms $O3^-$, ring atoms O2 connecting two neighboring Si atoms in 4-membered (4R) rings, and the bridging atoms O1 connect two neighboring 4R-rings forming the 8R-rings. Therefore, silicate sheets of apophyllites have regular 4R-rings that are connected to form distorted 8R-rings in the (001) plane. Cations (K^+, Ca^{2+}), anions (F^-, OH^-) and H_2O molecules are distributed between silicate layers.

The stability of apophyllites at high pressure, which has not been previously studied, is interesting for the following three reasons. First, the apophyllite structure consisting of pure silicate sheets is expected to remain stable to high pressures. Second, the apophyllite structure may be considered as a combination of several sublattices: water, anion–cation and silicate. Third, apophyllites, like zeolites and serpentines, are common minerals in hydrated oceanic basalts and hence are expected to play important roles in subduction zones. A detailed Raman spectroscopic investigation would allow us to describe the behavior of apophyllites (and each of its sublattices) at high pressures, including possible crystalline transitions, disordering and amorphization.

In the present work, we studied the evolution of single-crystal Raman spectra of OH- and F-apophyllites at hydrostatic and nonhydrostatic (quasi-hydrostatic, with addition of uniaxial loading along *c*-axis) compressions up to ~8 GPa. Considerable differences in the behavior of several bands observed in these two types of experiments demonstrate a high sensitivity of apophyllites to nonisotropic pressure and shear mechanical stresses.

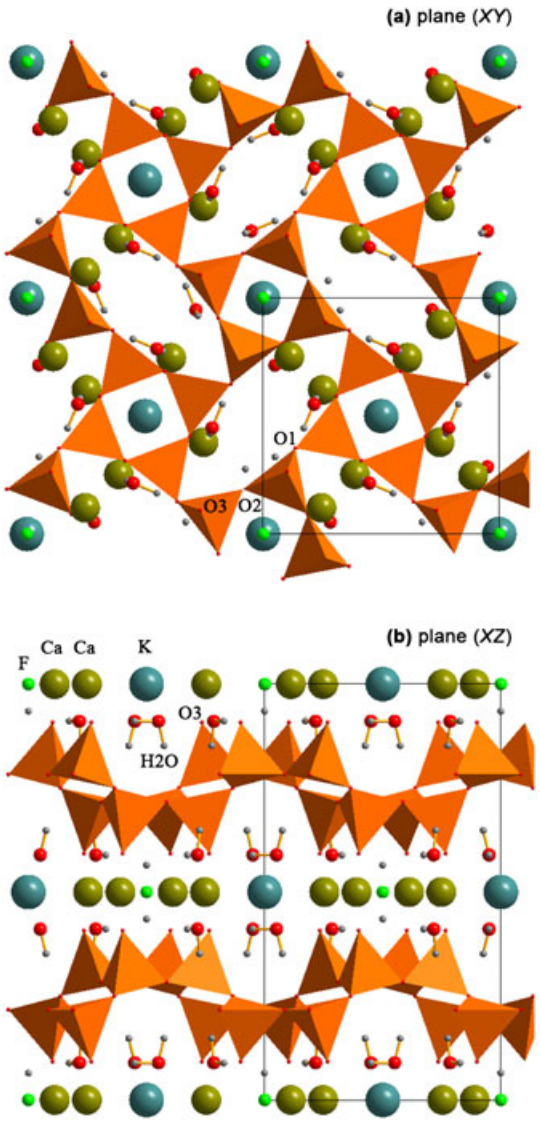

Figure 1. Crystal structure of F-apophyllite viewed down [001] (above) and [010] (below).

Materials and Methods

Single crystals of natural OH- and F-apophyllites with approximately end-member compositions from the University of Saskatchewan reference mineral collection were used in this study. These crystals had been characterized by electron microprobe analysis and Fourier transform infrared spectroscopy in the previous electron paramagnetic resonance studies of Mao and Pan[12] and Mao *et al.*[13] For each single crystal spectra were taken along all 3 axis using the Raman micro-probe at 30 points to verify the homogeneity of the sample.

Hydrostatic pressure was obtained in a diamond anvil cell (DAC), using a 0.2-mm stainless steel gasket (with 0.3 mm drilled hole) and a liquid medium (methanol–ethanol, 4 : 1). Pieces of ruby were placed in the medium of DAC. The pressure was determined from the shift in the ruby R_1 luminescence band (precision ±0.05 GPa).[14] Single crystals with large surface areas along the cleavage plane (001) were selected and put in DAC (orientation: *c*-axis is parallel to the DAC axis). Nonhydrostatic compression was produced by additional loading of uniaxial stress along *c* by means of contact with diamond surfaces. However, the absolute value of the uniaxial stress is unknown because no theoretical model has been developed to describe this complex mechanical compression of oriented crystals in DAC.

Journal of RAMAN SPECTROSCOPY

Raman spectra were recorded on a triple-grating Horiba Jobin Yvon T64000 Raman spectrometer equipped with an N_2-cooled charge coupled device detection system in subtractive dispersion mode.[15] The slits were set for a spectral resolution of 2 cm^{-1}. Radiation of 514.5 nm from an argon ion laser power 50 mW on the sample was used. An Olympus microscope lens with the focal distance $f = 10.6$ mm and numerical aperture NA = 0.5 was used to focus the laser on the sample. Complex bands were deconvoluted into Voigt contours using PeakFit (Systat Software Inc.) software package.

Results and Discussion

Raman spectra of OH-apophyllite at nonhydrostatic pressures are presented in Fig. 2. This nonhydrostatic behavior differs from that of OH-apophyllite compressed at hydrostatic conditions, shown in Fig. 3.

Wavenumbers of peaks (ν) of OH-apophyllite compressed in hydrostatic and nonhydrostatic conditions are monotonously shifted with pressure (Fig. 4). In decompression, the changes in Raman spectra of OH-apophyllite appear to be reversible, with hysteresis. Raman spectra of F-apophyllite are similar to those of its OH counterpart (Fig. 5), and the pressure dependences of peak wavenumbers for most bands are approximately linear (Fig. 6).

All modes in the centrosymmetrical structure of apophyllites are divided into g and u types. Optical g-modes are: $21A_{1g} + 22A_{2g} + 22B_{1g} + 21B_{2g} + 41E_g$, of them A_{1g}, B_{1g}, B_{2g}, E_g are Raman active. Optical u-modes are: $22A_{1u} + 23A_{2u} + 20B_{1u} + 21B_{2u} + 47E_u$, of them $A_{2u}(T_z)$ and E_u (T_x, T_y) are IR active. Lazarev[16], on the basis of vibrational analysis and IR data, interpreted apophyllite IR bands as vibrations of ν_s(SiOSi)-cycle, ν_{as}(SiOSi)-bridge etc. Using the lattice-dynamical computation program,[17] we have calculated F-apophyllite modes and the

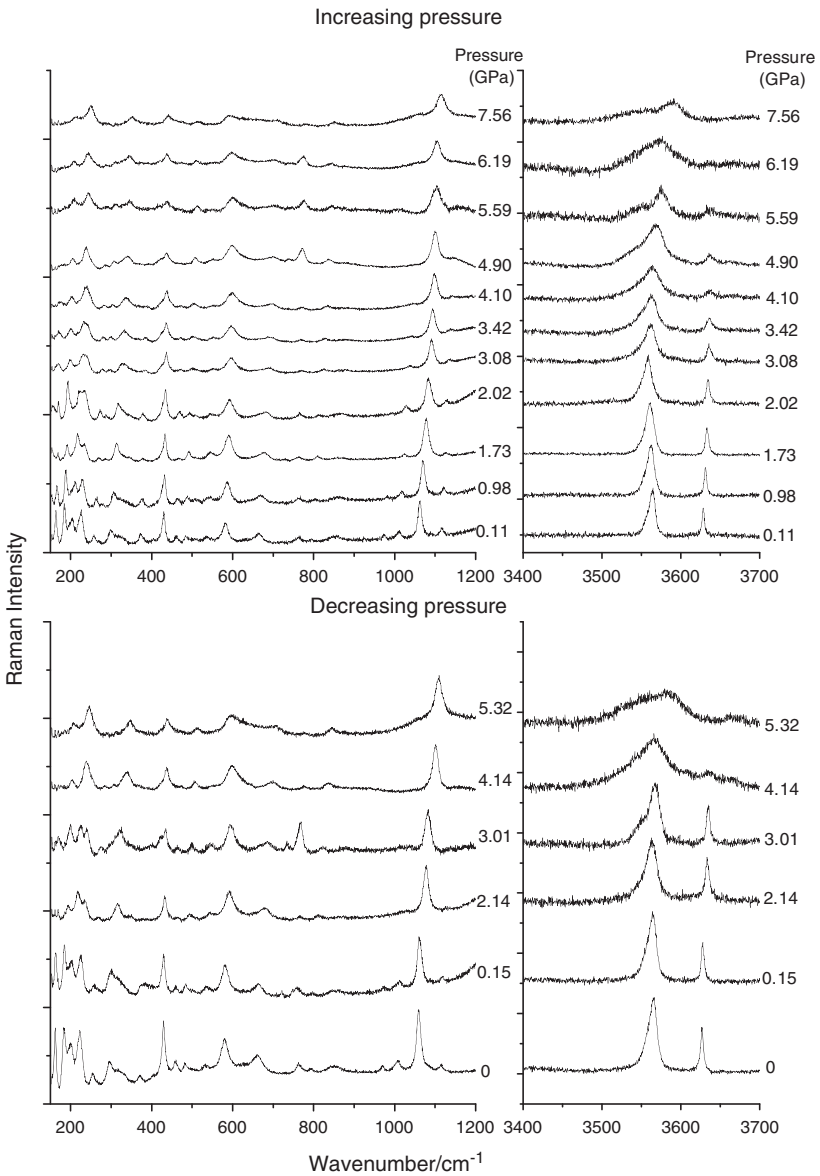

Figure 2. Raman spectra of OH-apophyllite collected at increasing and decreasing nonhydrostatic pressure (at room temperature).

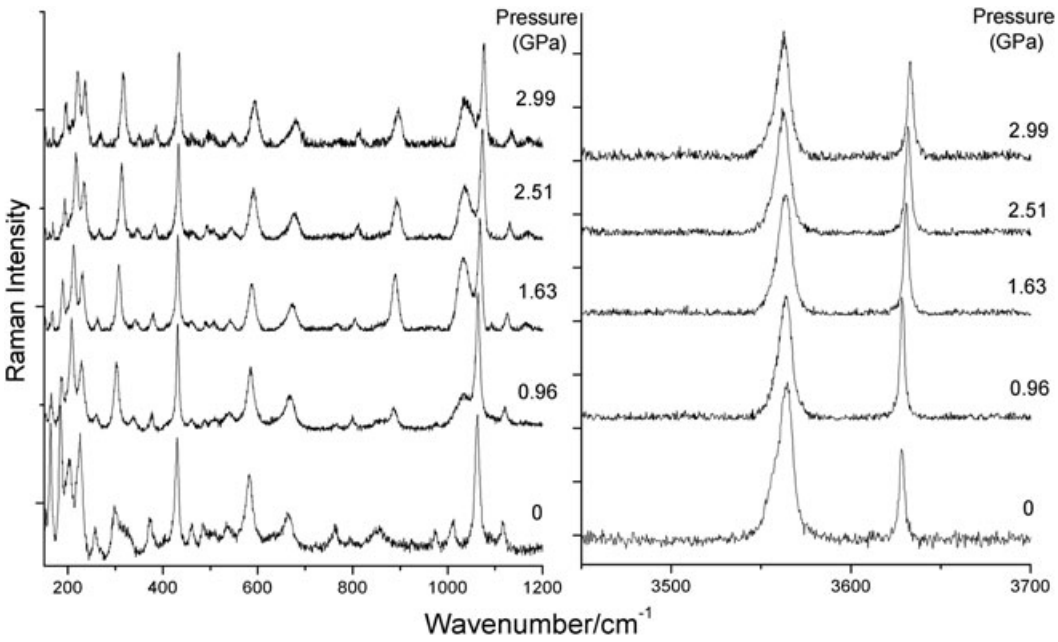

Figure 3. Raman spectra of OH-apophyllite at increasing hydrostatic pressure and room temperature.

obtained wavenumbers are given in Table 1, intensities and eigenvectors in Fig. 7. Our interpretation is generally similar to that in Ref.[18] for modes involving vibrations of bridge O1, 4R-cycle O2 and tail O3 oxygen atoms.

Below, we discuss every reliably detected Raman band in OH- and F-apophyllites and their baric behavior. The intense OH^- band at 3627 cm^{-1} in OH-apophyllite compressed hydrostatically exhibits a linear dependence of the wavenumber peak position on *P*. This band at nonhydrostatic compression shows a higher slope of the curve $\nu(P)$ with a negative curvature. The positive slope $d\nu/dP > 0$ of the band at 3627 cm^{-1} proves the decreasing H-bond energy and so the increasing bond length of this hydroxyl group OH^- with the silicate layers at high-*P*.

The intense O–H band at 3565 cm^{-1} of water molecules in OH-apophyllite shows a small negative slope $d\nu/dP < 0$ at the onset of compression. This band in F-apophyllite at 3558 cm^{-1} exhibits the same small negative slope $d\nu/dP < 0$, with a positive curvature (Fig. 6).

Above 6 GPa, OH-apophyllite compressed at nonhydrostatic conditions shows a nonlinear curve $\nu(P)$ for the band at 3565 cm^{-1}, with a large increase in wavenumbers of this O–H stretching band of H_2O (Fig. 4). The increase in wavenumber confirms a decreasing H-bond energy and increased distances between the H-bonded H_2O molecules. This process and strong broadening O–H bands are connected with amorphization observed at 6–7.5 GPa.

The band at 1117 cm^{-1} in OH-apophyllite exhibits HP-behavior with a remarkable slope $d\nu/dP$. The band at 1059 cm^{-1} shows a complex HP-behavior: the wavenumber of this band at nonhydrostatic compression strongly deviates from that at hydrostatic compression. This 1059 cm^{-1} band in OH-apophyllite has a significant slope $d\nu/dP$. Similarly, the 1062 cm^{-1} band in F-apophyllite has a significant slope $d\nu/dP$ at compression in hydrostatic medium.

The weak band at 1008 cm^{-1} in OH-apophyllite at nonhydrostatic conditions exhibits a pronounced slope $d\nu/dP$, which is similar at compression and decompression. This band is not observed in F- and OH-apophyllite at hydrostatic compression, being obscured by the parasitic band of the alcohol medium.

The weak band at 970 cm^{-1} has a positive slope $d\nu/dP$, which is similar for hydrostatic and nonhydrostatic compression of OH-apophyllite. This band intensity decreases with *P*. The band disappears at a pressure of about 4 GPa and was not observed at hydrostatic compression of F-apophyllite.

The pressure dependence of the weak and very broad band at 853 cm^{-1} exhibits a positive slope $d\nu/dP$, which is similar for hydrostatic and nonhydrostatic compression of OH-apophyllite. This band decreases in intensity and broadens with increasing *P*.

The low-intensity band at 793 cm^{-1} exhibits a nearly linear dependence of peak position on pressure, with a positive slope $d\nu/dP$, which is similar for hydrostatic and nonhydrostatic compression of OH-apophyllite. The band at 762 cm^{-1} in OH-apophyllite has a nearly linear dependence of peak position on pressure, with a nonpronounced slope $d\nu/dP$, similar under hydrostatic and nonhydrostatic compression.

The band at 662 cm^{-1} in OH-apophyllite shows a slightly nonlinear dependence of wavenumber peak position versus *P* with a small negative curvature. This band has a similar large slope $d\nu/dP$ for both hydrostatic and non-hydrostatic conditions.

The high-intensity band at 580 cm^{-1} in OH-apophyllite shows a strongly nonlinear dependence of wavenumber peak position versus *P* (above 4 GPa) with a negative curvature. This band shows a variable slope $d\nu/dP$, depending on pressure. The slopes of the curves for hydrostatic and non-hydrostatic conditions are similar coincide at low-*P* ($P < 3$ GPa). However, at non-hydrostatic compression above 6 GPa, the $d\nu/dP$ slope becomes negative.

The low-intensity band at 534 cm^{-1} in OH-apophyllite has an approximately (with scatter) linear dependence of peak wavenumber $\nu(P)$. This band decreases continuously in intensity with *P* and vanishes at ~5 GPa. Its band dependence $\nu(P)$ has a small slope $d\nu/dP$, which is similar for hydrostatic and nonhydrostatic compression. There is a hysteresis for nonhydrostatic compression.

Journal of RAMAN SPECTROSCOPY

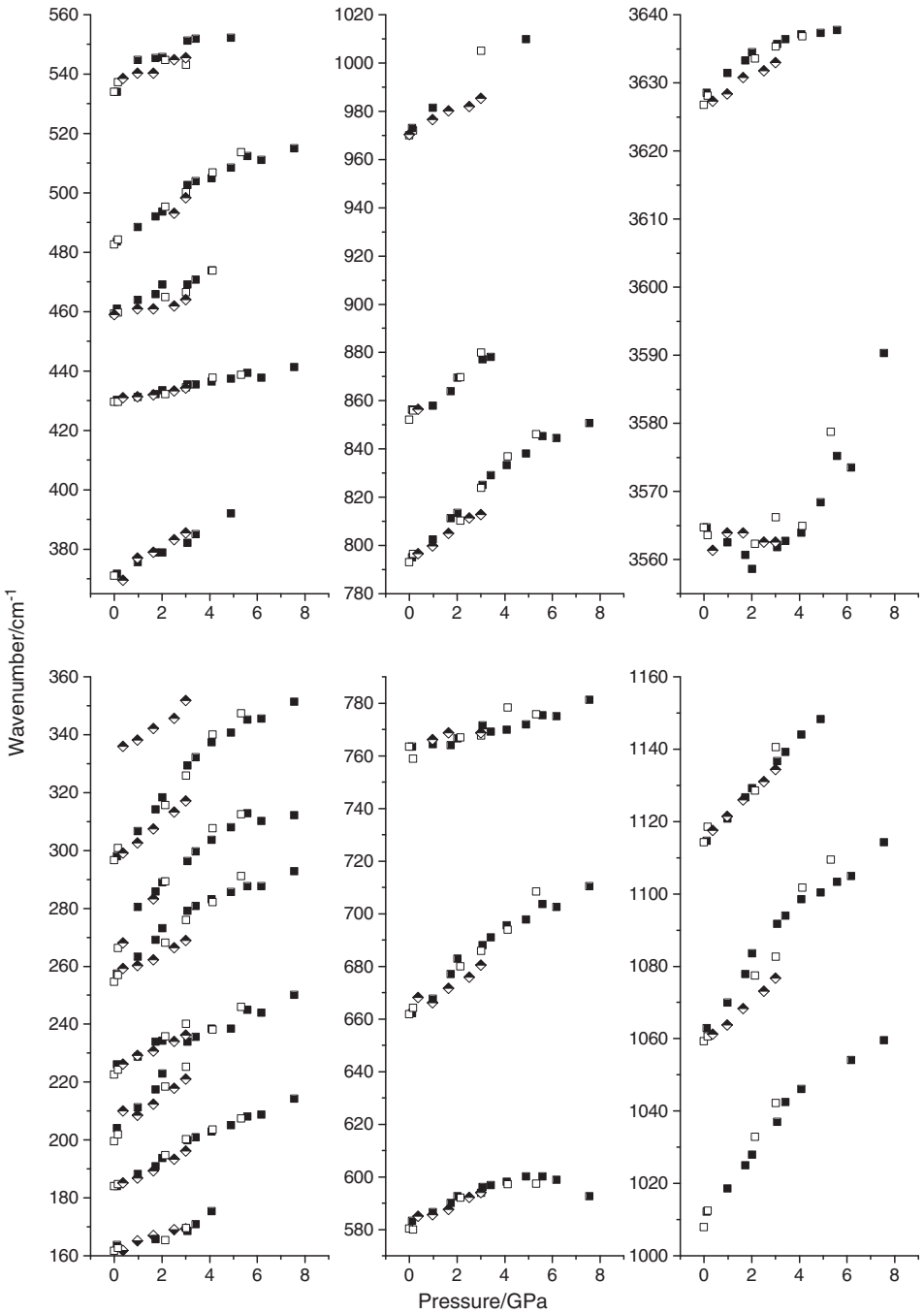

Figure 4. Pressure dependence of wavenumbers of Raman bands of OH-apophyllite at increasing (black squares) and decreasing (open squares) nonhydrostatic pressure and also at increasing hydrostatic pressure (black–white rhombs).

The peak wavenumber dependence $\nu(P)$ of the low-intensity band at 483 cm^{-1} is an approximately straight line, with a small negative curvature. The slope $d\nu/dP$ is similar for hydrostatic and nonhydrostatic regimes (Table 1).

The low-intensity band at 459 cm^{-1} in OH-apophyllite has an approximately linear dependence of peak position $\nu(P)$. Its intensity decreases with P, and the band disappears at ~4.3 GPa. Note that the slope $d\nu/dP$ is positive at nonhydrostatic compression but barely negative at hydrostatic compression.

The high-intensity, narrow band at 430 cm^{-1} in OH-apophyllite exhibits a linear dependence of peak wavenumber $\nu(P)$ with a modest slope $d\nu/dP$, which is similar for hydrostatic and nonhydrostatic compression. The peak wavenumber dependence $\nu(P)$ of the low-intensity band at 371 cm^{-1} in OH-apophyllite is nearly linear. The slope $d\nu/dP$ is similar for hydrostatic and nonhydrostatic compression, without hysteresis. With increasing P, this weak band loses its intensity and disappears at ~5 GPa.

The band at 335 cm^{-1} in OH-apophyllite compressed hydrostatically has an approximately linear dependence of peak position $\nu(P)$. However, this band in OH-apophyllite compressed nonhydrostatically, is overlapped to the neighboring band at

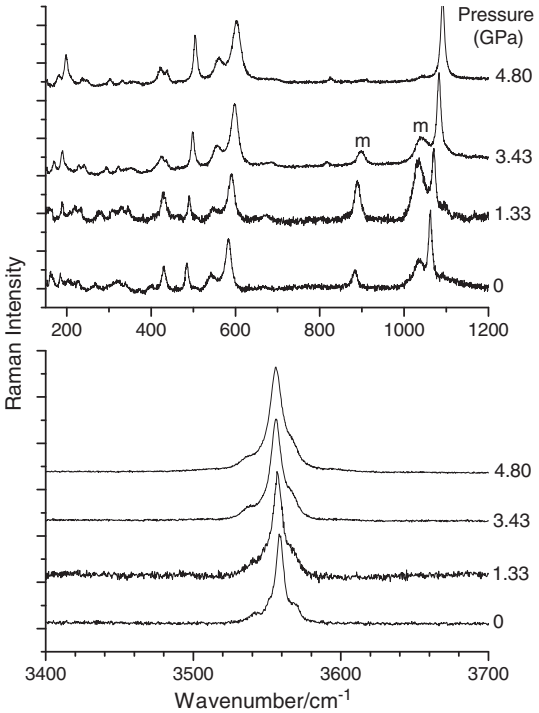

Figure 5. Raman spectra of F-apophyllite at increasing hydrostatic pressure and room temperature.

297 cm^{-1} and thus difficult to resolve (this band is not shown in Table 1).

The strong band at 297 cm^{-1} in OH-apophyllite exhibits different behavior between hydrostatic and nonhydrostatic compressions. Specifically, this band in OH-apophyllite compressed hydrostatically has an approximately linear dependence $\nu(P)$, whereas the curve $\nu(P)$ of this band at nonhydrostatic compression deviates significantly from a straight line, with a negative curvature. The intensity of this band increases slightly with P.

The weak bands at 255 and 266 cm^{-1} in OH-apophyllite compressed nonhydrostatically exhibit similar dependences $\nu(P)$ and probably have the same origin, i.e. as libration–translation motions of interconnected tetrahedra. The wavenumbers of these bands for crystals compressed hydrostatically show slightly lower values than those at nonhydrostatic compression.

The strong band at 223 cm^{-1} in OH-apophyllite exhibits an approximately linear dependence of peak wavenumber $\nu(P)$ with a nonpronounced slope $d\nu/dP$, which is similar for hydrostatic and nonhydrostatic compressions, i.e. this band is nonsensitive to deviations from hydrostacity.

The strong band at 200 cm^{-1} in OH-apophyllite exhibits an approximately linear (with scatter) dependence of peak wavenumber $\nu(P)$. The band curve $\nu(P)$ at nonhydrostatic compression deviates slightly from a straight line. The band at 200 cm^{-1} in OH-apophyllite compressed nonhydrostatically is broad and overlapped with the 223 cm^{-1} band at P above 3 GPa.

The strong narrow band at 185 cm^{-1} in OH-apophyllite shows a nearly linear dependence of peak wavenumber $\nu(P)$ with a small negative curvature. The average slope is similar for hydrostatic and nonhydrostatic compressions.

The high-intensity band at 162 cm^{-1} in OH-apophyllite has a nonlinear dependence of peak wavenumber $\nu(P)$ with a modest positive slope $d\nu/dP$, which decreases with P. The intensity of this band decreases quickly with P.

Raman spectra of F-apophyllite at high hydrostatic pressures are presented in Fig. 5. Wavenumbers of peaks are monotonously shifted with pressure (Fig. 6). For majority of the bands, each dependence $\nu(P)$ is describable with a linear function, except those of the bands at 3558, 668, 269 and 227 cm^{-1}.

The strong stretching O–H band at 3558 cm^{-1} of H_2O molecules in F-apophyllite exhibits a nonlinear dependence of peak wavenumber $\nu(P)$ with a negative slope $d\nu/dP$ and a positive curvature $d^2\nu/dP^2 > 0$. This dependence confirms the strengthening of the hydrogen bonds of the H_2O molecules with the silicate sheets.

With increasing P, the majority of the bands in F-apophyllite are shifted with similar slopes to those in OH-apophyllite compressed hydrostatically (Table 1). However, the band at 430 cm^{-1} in OH- and F-apophyllites has a different behavior. In particular, this mode in F-apophyllite exhibits a splitting into two components of approximately equal intensities increasing with P. This mode in OH-apophyllite splits into two components of different intensities, where the smaller component is difficult to locate accurately.

Interpretation of the observed modes, according to our calculations of lattice dynamics of F-apophyllite, is presented in Table 1. Observed bands are assigned to O–H stretching, Si–O stretching, SiO_4 bending internal modes and external vibrations (translations and librations) of tetrahedrons, H_2O librations and also translations of cations, anions and H_2O molecules. Our interpretation of the modes in apophyllites (Table 1) is broadly similar to that of McKeown *et al.*[18] for micas.

Among the stretching and bending modes of SiO_4, we can distinguish the modes of different oxygen atoms: 4R-ring O2, bridge O1 and tail $O3^-$ (Table 1). Atoms O2, O1 and Si form the 8R-rings. Interlayer translation modes of ions and molecules have low wavenumbers, determined by weak force constants, which strongly depend on interatomic distances controlled by interlayer volume. These modes should be more sensitive to nonhydrostatic compression with additional stress along c, when volume between the silicate sheets is decreased and the coordination polyhedra of these atoms are strongly deformed. The stretching modes of $Si–O3^-$, oriented closely to c-axis, could be also sensitive to this nonhydrostatic compression.

Our interpretation of the modes can explain the complex behavior of some bands at nonhydrostatic compression, which differs from that observed at hydrostatic compression. Such difference is observed for bands at 3627, 1059, 662, 459, 297 and 255 cm^{-1} in OH-apophyllite.

At hydrostatic compression, the band wavenumbers of F- and OH-apophyllites show linear dependences $\nu_h(P)$, whereas at nonhydrostatic compression, the wavenumbers of many bands follow nonlinear dependences $\nu_{nh}(P)$ with hysteresis.

In the case of hydrostatic compression, crystalline states of F- and OH-apophyllites are retained up to the maximum measured pressure of 5 and 3.2 GPa, respectively. In particular, the intensities of Raman bands do not decrease with P. Also, the band widths do not increase with P either. These data demonstrate the absence of amorphization of apophyllites at hydrostatic compression in the P-range investigated.

Amorphization was observed in spectra of OH-apophyllite compressed nonhydrostatically. The OH bands at 3565 and 3627 cm^{-1} are particularly sensitive to nonhydrostatic condition and increasing disordering. Their intensities decrease and their band widths significantly increase with pressure. For example,

Journal of RAMAN SPECTROSCOPY

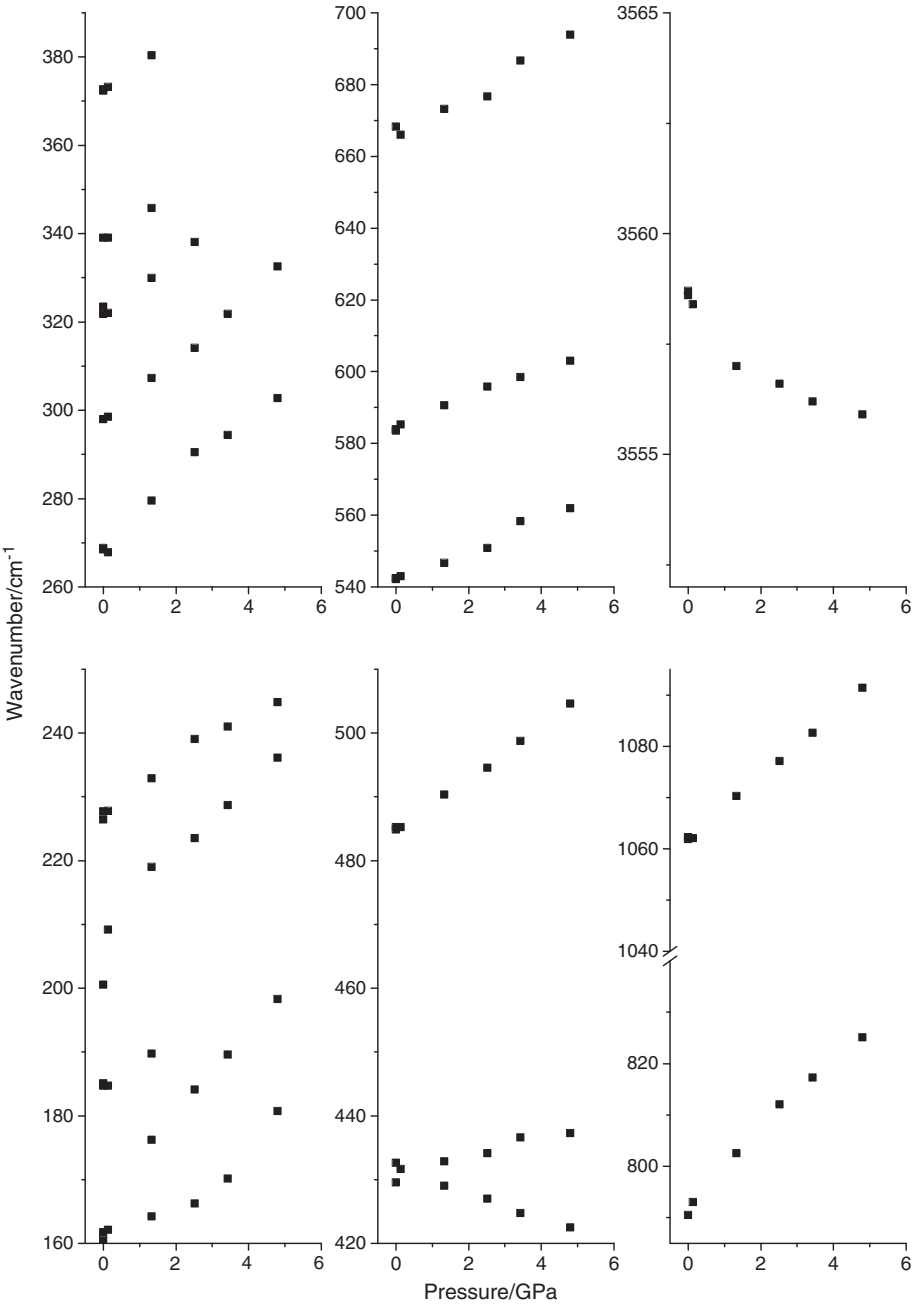

Figure 6. Pressure dependence of wavenumbers of Raman bands of F-apophyllite at increasing (black squares) hydrostatic pressure.

the OH stretching bands are broadened by 2.5 times when pressure is increased to ~7 GPa. Also, the intensity of the hydroxyl mode at 3627 cm^{-1} decreases at 3–6 GPa and this band disappears at 6.2 GPa.

Nonhydrostatic conditions give rise to considerable changes in the low-wavenumber range of the Raman spectra that can be linked to disordering of ions (cations and anions) and molecules H_2O in the interlayer region. Integral intensity of all low-wavenumber bands ($\nu < 200\ cm^{-1}$) observed in Fig. 2 is decreased with nonhydrostatic compression that should be associated with loss of peak intensity and broadening these translation bands. Two initially narrow bands at 162 and 200 cm^{-1} in OH-apophyllite disappear at nonhydrostatic conditions of compression at about ~3–4 GPa. Both modes are associated with joint vibrations of interlayer cations Ca^{2+} and H_2O (Table 1).

The vibrational modes of ions and molecules in the interlayer region are sensitive to additional compression along the *c*-axis. Moreover, OH^- and H_2O groups are highly sensitive to this additional compression due to the highly sensitive nature weak H-bonds have to the deformation of coordination polyhedra. Furthermore, hydroxyl groups in OH-apophyllite are oriented along the *c*-axis, and Ca–OH_2 bonds are aligned closely to the *c* axis and this may cause broadening of the internal O-H

Table 1. Vibrational bands of OH- and F-apophyllite and their assignments

ν	ν'_h	ν'_{nh}	ν'_{nh}	ν	ν'_h	ν	
OH- apo.	OH- apo. hyd.	OH-apo. non-h. P_{up}	OH-apo. non-h. P_{down}	F-apo.	F-apo. hyd.	F-apo. calc., symm.	Interpretation of F- and OH-apo. bands
							stretch(O–H):
3627	2.16	3.25	2.03				$\nu(OH^-)$
3565	0.12	−2.98	−0.93	3558	−0.61	3566 A_{1g}	ν_{as}(HOH), ν_s(HOH)
							stretch(SiO_4):
1117	6.34	7.17	7.66	1116	—	1105 E_g	ν_{as}(Si–O2–Si)
1059	5.91	6.67	9.59	1062	6.18	1084 A_{1g}	$\nu(SiO3^-)$
1008	—	8.55	11			1033 A_{1g}	ν_{as}(Si–O2–Si)
						1003 E_g	$\nu(SiO3^-)$
970	—	7.56	13.88			1000 E_g	$\nu(SiO3^-)$
							***F*-bend(SiO_4) + *R*(H_2O)**:
852[a]	—	10.39	10.38	856	—	882 A_{1g}	breath(Si_4)[b] + ν_s(Si–O2–Si)+ ν_s(Si–O1–Si)
793	6.49	9.2	10.05	790.5	7.2	738 A_{1g}	$R(H_2O) + \nu_s$(Si–O1–Si)
762	1.09	2.3	3.15	768	—	679 A_{1g}	$R(H_2O) + \delta(SiO3^-)$
							***E*-bend(SiO_4) + *R*(H_2O)**:
662	5.03	8.6	8.3	668	5.3	658 A_{1g}	δ(Si–O1–Si) + $\delta(SiO3^-)$+ collapse(Si_8O_8) + breath($O2_4$)
580	3.63	4.74	3.59	584	3.97	625 A_{1g}	breath($O2_4$) + $\delta(SiO3^-)$
534	2.78	3.5	3.04	542.3	4.22	—	—
483	4.4	5.32	5.76	485	4.13	556 A_{1g}	collapse(Si_8O_8) + breath(Si_4O2_4)
							ext(SiO_4) + *TR*(H_2O) + *T*(ions):
459	—	3.0	3.2	464	—	—	—
				431.6	−1.79	404 A_{1g}	$T_{xy}(H_2O) + \delta(SiO3^-)$
430	1.23	1.45	1.81	430.1	1.7	—	—
371	5.51	4.07	—	373	5.96	—	—
335	5.67	—	—	339	5.1	—	—
				322	6.03	—	—
297	6.86	10.15	9.57	298	7.37	292 A_{1g}	$R(O1–O3^-) + T_{xy}(Ca^{2+})$
266	—	7.57	9.11	266.8	7.27	—	—
255	4.73	7.9	6.71				
							***T*(ions) + *T*(H_2O)**:
223	3.63	2.98	5.77	227.6		223 A_{1g}	$T_{xy}(Ca^{2+})$
200	4.63	9.37	8.76	209.2	5.0	210 E_g	$T_z(Ca^{2+}) + T_{xyz}(H_2O)$
185	4.16	4.02	4.53	184.7	3.53	178 A_{1g}	$T_z(Ca^{2+}) + T_z(H_2O)$
162	2.74	2.67	2.23	160.5	2.56	165 A_{1g}	$T_{xy}(Ca^{2+}) + T_{xy}(H_2O)$
132.3	—	—	—	131.6	—	—	—
105	—	—	—	105.5	—	107 A_{1g}	$T_{xy}(Ca^{2+}) + T_{xy}(H_2O)$

Our experimental and calculated Raman spectra are given: peak position ν (cm^{-1}) and rate ν' (cm^{-1} GPa^{-1}) of band shift with pressure. Data of hydrostatic (hyd.) and nonhydrostatic (non-h.) compression are used.

[a]Wide band.

[b]Symmetric breathing mode of 4Ring(Si_4).

apo., apophyllite; ***E***- and ***F*-bend**, bending modes originated from *E* and *F* symmetry modes of 'free' tetrahedron SiO_4; T_z, translation mode along the direction noted; **ext**, external modes (*R* – librations, *T* – translations, *TR* – both) of a group; **stretch** ν, ν_s and ν_{as}, stretching modes (nonsym metric, symmetric and asymmetric ones in SiOSi and HOH bridges); δ, deformation mode along the normal to the bridge plane or to the bond.

stretching and external translation vibrations of noted groups when compression increases along *c*-axis.

Conclusion

The present study shows for the first time that Raman spectra of natural F- and OH-apophyllites exhibit continuous changes (mainly in the peak positions) with increasing hydrostatic pressure. The observed intensities and widths of these Raman bands confirm that apophyllites remain crystalline at hydrostatic pressures up to at least ~5 GPa.

At nonhydrostatic compression, the intensities for the majority of the bands in OH-apophyllite decrease with *P*, and several bands vanish at about 3–5 GPa. There is a hysteresis for nonhydrostatic compression. The pronounced changes in the intensities and widths of Raman bands reflect the amorphization process of apophyllites induced by nonhydrostatic compression.

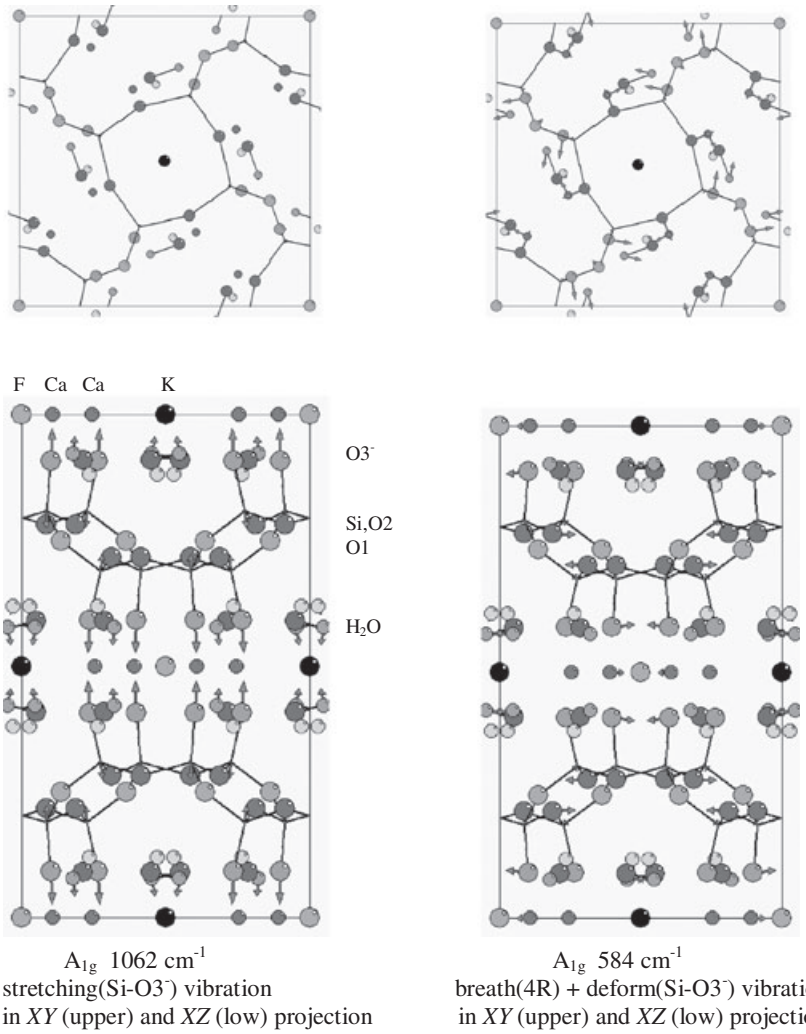

A_{1g} 1062 cm^{-1}
stretching(Si-$O3^-$) vibration
in *XY* (upper) and *XZ* (low) projection

A_{1g} 584 cm^{-1}
breath(4R) + deform(Si-$O3^-$) vibration
in *XY* (upper) and *XZ* (low) projection

Figure 7. Calculated eigenvectors of atom vibrations for bands at 1062 and 584 cm^{-1} of F-apophyllite crystal viewed down [001] and [010]. Atom radii in [001] projection are plotted in 2 times smaller than those in [010] projection.

Acknowledgements

This work was supported by the Siberian Division of RAS (Integration Project 109), the Russian Ministry of Science and Education and the CRDF (BRHE - REC-008 grant) and the Russian Foundation for Basic Research (RFBR-11-05-01121).

References

[1] J. Badro, J. L. Barrat, Ph. Gillet, *Phys. Rev. Lett.* **1996**; *76*, 772.
[2] J. Haines, J. M. Léger, C. Chateau, *Phys. Rev. B.* **2000**; *61*, 8701.
[3] J. Haines, J. M. Léger, F. Gorelli, M. Hanfland, *Phys. Rev. Lett.* **2001**; *87*, 155503.
[4] K. J. Kingma, R. J. Hemley, H. K. Mao, D. R. Veblen, *Phys. Rev. Lett.* **1993**; *70*, 3927.
[5] L. E. McNeil, M. Grimsditch, *Phys. Rev. Lett.* **1992**; *68*, 83.
[6] M. B. Kruger, R. Jeanloz, *Science* **1990**; *249*, 647.
[7] Y. Tsuchida, T. Yagi, *Nature* **1990**; *347*, 267.
[8] A. K. Kleppe, A. P. Jephcoat, *Mineralogical Mag.* **2004**; *68* (3), 433.
[9] P. J. Dunn, R. C. Rouse, J. A. Norberg, *Am. Mineral.* **1978**; *63*, 196.
[10] G. Brocardo, Minerals & Gemstones of the World, David & Charles Book, London, **1994** .
[11] K. Ståhl, Å. Kvick, S. Ghose, *Acta Cryst.* **1987**; *B43*, 517.
[12] M. Mao, Y. Pan, *Eur. J. Mineral.* **2009**; *21*, 317.
[13] M. Mao, M. J. Nilges, Y. Pan, *Eur. J. Mineral.* **2010**; *22*, 89.
[14] R. G. Munro, G. J. Piermarini, S. Block, W. B. Holzapfel, *J. Appl. Phys.* **1985**; *57*(2), 165.
[15] V. S. Minkov, A. S. Krylov, E. V. Boldyreva, S. V. Goryainov, S. N. Bizyaev, A. N. Vtyurin, *J. Phys. Chem. B.* **2008**; *112*, 8851.
[16] A. N. Lazarev, Vibrational spectra and construction of silicates, Nauka, Leningrad, **1968**. (in Russian)
[17] M. B. Smirnov, A. P. Mirgorodsky, P. Quintard, *J. Mol. Structure* **1995**; *348*, 159.
[18] D. A. McKeown, M. I. Bell, E. S. Etz, *Am. Mineral.* **1999**; *84*, 1041.